

Neutral Hydrogen and Its Emission Lines in the Solar Corona

Jean-Claude Vial & Martine Chane-Yook

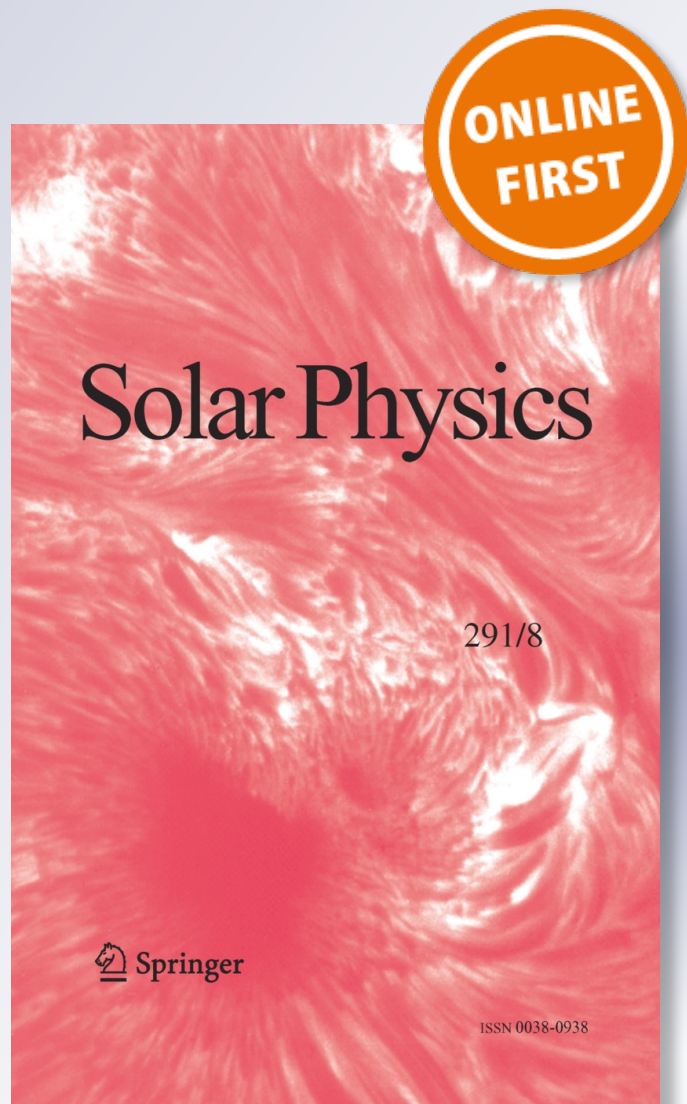
Solar Physics

A Journal for Solar and Solar-Stellar
Research and the Study of Solar
Terrestrial Physics

ISSN 0038-0938

Sol Phys

DOI 10.1007/s11207-016-0995-x



Your article is protected by copyright and all rights are held exclusively by Springer Science +Business Media Dordrecht. This e-offprint is for personal use only and shall not be self-archived in electronic repositories. If you wish to self-archive your article, please use the accepted manuscript version for posting on your own website. You may further deposit the accepted manuscript version in any repository, provided it is only made publicly available 12 months after official publication or later and provided acknowledgement is given to the original source of publication and a link is inserted to the published article on Springer's website. The link must be accompanied by the following text: "The final publication is available at link.springer.com".

Neutral Hydrogen and Its Emission Lines in the Solar Corona

Jean-Claude Vial¹  · Martine Chane-Yook¹

Received: 8 March 2016 / Accepted: 16 September 2016
© Springer Science+Business Media Dordrecht 2016

Abstract Since the Lyman- α rocket observations of Gabriel (*Solar Phys.* **21**, 392, 1971), it has been realized that the hydrogen (H) lines could be observed in the corona and that they offer an interesting diagnostic for the temperature, density, and radial velocity of the coronal plasma. Moreover, various space missions have been proposed to measure the coronal magnetic and velocity fields through polarimetry in H lines. A necessary condition for such measurements is to benefit from a sufficient signal-to-noise ratio. The aim of this article is to evaluate the emission in three representative lines of H for three different coronal structures. The computations have been performed with a full non-local thermodynamic-equilibrium (non-LTE) code and its simplified version without radiative transfer. Since all collisional and radiative quantities (including incident ionizing and exciting radiation) are taken into account, the ionization is treated exactly. Profiles are presented at two heights (1.05 and 1.9 solar radii, from Sun center) in the corona, and the integrated intensities are computed at heights up to five solar radii. We compare our results with previous computations and observations (e.g. $L\alpha$ from *Ultraviolet Coronal Spectrometer*) and find a rough (model-dependent) agreement. Since the $H\alpha$ line is a possible candidate for ground-based polarimetry, we show that in order to detect its emission in various coronal structures, it is necessary to use a very narrow (less than 2 Å wide) bandpass filter.

Keywords Sun corona · Hydrogen lines · Non-LTE diagnostics

1. Introduction

It came as a surprise to discover that a hot and diluted medium such as the corona was emitting the “cool” Lyman- α ($L\alpha$ from now on) line (Gabriel, 1971). Since this rocket observation (in an eclipse), many more $L\alpha$ observations have been performed (e.g. Hassler *et al.*, 1994 and Kohl *et al.*, 1995 by the *Ultraviolet Coronal Spectrometer* (UVCS) on board

✉ J.-C. Vial
jean-claude.vial@ias.u-psud.fr

¹ Institut d’Astrophysique Spatiale, CNRS, Université Paris-Sud, Université Paris-Saclay, Bât. 121, 91405 Orsay cedex, France

Spartan, and later on by the *Ultraviolet Coronal Spectrometer* (UVCS) on board the *Solar and Heliospheric Observatory* (SOHO) (Zangrilli *et al.*, 1999 and Maccari *et al.*, 1999)) with the help of a coronagraph. The emission was quickly identified as the resonance scattering of the chromospheric $\text{L}\alpha$ radiation by “trace” neutral hydrogen (usually taken as about 10^{-6} electron density). Because $\text{L}\alpha$ is the strong resonance line of the most abundant element (hydrogen) and because the emitted chromospheric profile is about as wide as the absorption profile of coronal neutral hydrogen, in the absence of a velocity field, the emission is rather strong (about 10^{-6} the disk value at $1.5 R_{\odot}$) and even stronger (a few 10^{-5}) in a streamer (*e.g.* Miralles *et al.*, 1999). This is why a major future mission, *Solar Orbiter*, includes the $\text{L}\alpha$ coronagraph called *Multi Element Telescope for Imaging and Spectroscopy* (METIS) (Antonucci *et al.*, 2012). Moreover, it has been shown as early as 1982 (Bommier and Sahal-Brechot, 1982) that the line was sensitive to the Hanle effect (generally effective in weak magnetic fields). Consequently, many (space) projects have proposed polarimetric measurements in this line (*e.g.* the *Small Explorer for Solar Eruptions* (SMESE) mission (Vial *et al.*, 2007) and more recently the *Coronal Ultraviolet Spectro-Polarimeter* (CUSP) on board the *Solar magnetism eXplorer* (SolmeX) (Peter *et al.*, 2012), the *MAGnetic Imaging Coronagraph* (MAGIC) on board the *INvestigation of Solar-Terrestrial Activity aNd Transients* (INSTANT) mission (Lavraud *et al.*, 2015, proposal to ESA), the *MAGnetic Imaging Coronagraph* (MAGIC) on board the *Magnetic Activity of the Solar Corona* (MASC) mission (Auchère *et al.*, 2015, proposal to ESA). It has also been proposed to use the Lyman- β ($\text{L}\beta$ from now on) line for performing polarimetric measurements in the faint corona (Peter *et al.*, 2012).

However, until now, these projects are still at the proposal level for various reasons including the (relative) complexity of the instrumentation and the fact that polarimetry is “photon-hungry” and requires large apertures in the ultraviolet (UV). Apart from radio observations above active regions, another path toward coronal polarimetry has been pursued with ground-based infrared (IR) observations measuring the Zeeman effect (Lin, Penn, and Tomczyk, 2000; Tomczyk *et al.*, 2008).

Another possibility has been opened with eclipse polarization measurements in red and green channels by Kim *et al.* (2013b) from which these authors concluded that “the polarization excess (green–red) can be explained by the presence of neutral hydrogen in the corona” (see also Dolei *et al.*, 2014). As mentioned by Kim *et al.* (2013b), Poland and Munro (1976) and Mierla *et al.* (2011) had already concluded that $\text{H}\alpha$ contributed to coronagraphic images of transients and coronal mass ejections (CMEs), respectively. Actually this was demonstrated with eclipse measurements made at the *Canada–France–Hawaii Telescope* (CFHT) in 1991 where Vial *et al.* (1992) detected a plasmoid in the solar corona that Koutchmy *et al.* (1994) interpreted as emitting essentially in the $\text{H}\alpha$ line, a claim discussed later on by Zhukov *et al.* (2000) who proposed an upper limit of the emission of about 2 % of the background corona. Moreover, the Hanle effect has been successfully used in the $\text{H}\alpha$ line, in spite of its optical thickness, in magnetic-field measurements in prominences (*e.g.* Leroy, 1981; Bommier, Sahal-Brechot, and Leroy, 1981).

In order to derive the plasma properties (including magnetic field) it is imperative to take into account all processes involved and first of all the proper ionization degree. The aim of this work is to compute most observable parameters (line profile, intensity) for the main H lines exactly emitted by (three) typical regions of the solar corona and at various heights above the limb.

In Section 2, we present the full non-local thermodynamic-equilibrium (non-LTE) computations derived from 1D non-LTE codes which are adapted to the geometry of the corona. In Section 3, we focus on profiles obtained in the $\text{L}\alpha$, $\text{L}\beta$, and $\text{H}\alpha$ lines at various heights.

In Section 4, we also compare with other computational and observational results in the $L\alpha$ and $L\beta$ lines. In Section 5, we provide the variation with altitude of the ionization degree for the three models. In Section 6, we discuss all our results, and we pay some attention to the possibility of observing the $H\alpha$ line in the corona. In Section 7, we conclude on further improvements in the computations.

We also present in the Appendix an approximation to obtain the $H\alpha$ intensity from the (measured) $L\alpha$ emission.

2. Non-LTE Computations

As far as hydrogen lines are concerned, we remark that the radiative output of structures such as prominences and the corona is dominated by the incident radiation and the resonance scattering as follows. The $L\alpha$ case has been extensively studied since the pioneering work of Heasley and Mihalas (1976) who built a non-LTE code adapted to one-dimensional cool layers located in the corona illuminated by the photospheric, chromospheric and coronal radiation. Much modeling has been performed since (*e.g.* Gouttebroze, Heinzel, and Vial, 1993) where the prominence was considered as an isothermal and isobaric layer. More recently, prominence–corona transition regions (PCTRs) have been grafted to the homogeneous layer on the basis of magnetohydrostatic (mhs) equilibrium by Anzer and Heinzel (1999) and then consistent mhs models of threads have been combined with the addition of inhomogeneous layers (Heinzel, Anzer, and Gunár, 2005); for comprehensive reviews of this modeling, see Labrosse *et al.* (2010), Gunár (2014), Labrosse (2015), and Heinzel (2015). In all these recent models, there is basically a cool core ($T \approx 10,000$ K) and a PCTR, where physical quantities vary drastically up to the corona itself where the density is low enough for all the lines and continua of all elements (including hydrogen) to be optically thin. In the low corona, the Lyman lines have been treated by Noci, Kohl, and Withbroe (1987) with the simple assumption of resonance scattering to begin with and later on with the inclusion of electron collisions, which allows for more information to be drawn from $L\alpha$ and $L\beta$ observations (Withbroe *et al.*, 1982; Raymond *et al.*, 1997). As shown by Labrosse, Li, and Li (2006) in the case of a coronal streamer, the $L\alpha$ line is essentially radiatively formed but the $L\beta$ line becomes increasingly collisionally driven with increasing altitude. Moreover, as discussed in Section 5, the ionization has been computed up to now within the simplified model of Gabriel (1971).

For various reasons (including its non-detection even with the best coronagraphs, the best seeing, and the most narrow filters), the coronal $H\alpha$ line has never been studied in detail. It is formed in the corona through various processes (radiative and partly collisional) involving at least the three first levels and possible cascades from higher levels including the continuum. In the Appendix, we propose a simple approach for computing $H\alpha$, an approach which involves radiative processes and the first three levels only.

In order to perform an exact computation of the hydrogen lines (which implies to compute a high number of population levels, including the continuum, with all processes taken into account), we decided to follow a “non-LTE radiative transfer” approach although it is clear that because of the low neutral density in the corona (about 10^{-6} times the electron density) all hydrogen lines are optically thin and all resonance scatterings are not followed by a second scattering. The advantage is that the bulk of the code is available and well controlled, in such a way that it is then possible to treat many hydrogen levels (including the continuum) with precise incident radiation altitude-dependent profiles which are critical for the population of H levels. This approach does not simplify the incident profiles, contrary

to Auchère (2005) or Dolei, Spadaro, and Ventura (2015), who use a combination of three gaussians. It formally allows for the consideration of incident profiles varying with distance to the limb, or with the presence of close active regions, or the variation with activity. As far as the thermodynamic parameters, density [n_e] and temperature [T_e] of the corona are concerned, they vary with radial distance (see Section 2.2). As already mentioned, such an approach has been followed by Labrosse, Li, and Li (2006) who computed the $L\alpha$ and $L\beta$ integrated intensities in a streamer defined by the three-fluid solar-wind model of Li, Li, and Labrosse (2006). However, we proceeded with a different method and different models as shown below.

2.1. The Computational Method

The initial prominence code, PROM5 (https://idoc.ias.u-psud.fr/MEDOC/Radiative_transfer_codes/PROM5) is modified as follows. Instead of a cool core with an extended PCTR, we simply have no layer with low temperature but only a so-called PCTR with actual coronal conditions in a spherically symmetric configuration where the density decreases from the impact parameter position toward both sides of the line-of-sight (LOS). The medium being optically thin in all lines and in all directions, the incident radiation is exactly computed at each radial distance. Actually, the computation of the $L\alpha$ line emitted when the line-of-sight crosses the limb (and where a plane-parallel LOS computation makes no sense) has been performed in the more difficult case of an optically thick atmosphere (Vial, 1970). In order to simplify the computations, we adopted the same model extension, for all line-of-sights located at altitudes between 1.05 and $5 R_\odot$. This means that the boundaries along each LOS are (symmetrically) defined by the last external layer of the radial model. Through extrapolation, we checked that the neglected (out-of-model) parts along the LOS did not contribute much to the computed opacities (*i.e.* intensities): for $L\alpha$ we found less than 1 % at $1.05 R_\odot$ and much less for the other lines and lower altitudes. For higher altitudes (*i.e.* $5 R_\odot$), the neglected opacity reaches 4 % for the coronal-hole model.

The dedicated coronal code, PROMCOR, is available at https://idoc.ias.u-psud.fr/MEDOC/Radiative_transfer_codes/PROMCOR, where a typical coronal-hole model is proposed as an input.

2.2. The Physical Models

We limited our study to three different models: the quiet-corona and polar coronal-hole models provided by Allen (1977) and the streamer model of Goryaev *et al.* (2014). The streamer model is provided in 2D as an angular diverging slab with a Gaussian shape with a constant temperature of 1.43×10^6 K, as derived from the measurements from the *Sun Watcher using Active Pixel System Detector and Image Processing* (SWAP) and the *Extreme Ultraviolet Imaging Spectrometer* (EIS) on board *Hinode*. We simplified the model into a spherically symmetric one with a temperature of 10^6 K in order to better compare with the quiet-corona values of Allen (1977). Note that Dolei, Spadaro, and Ventura (2015) found a temperature range of 5×10^5 K– 1.5×10^6 K between 2 and $6 R_\odot$, over a large range of position angles. We adopted the radial density provided by Equation (16) and Table 2 of Goryaev *et al.* (2014). In doing so, we do not have to take into account any background contribution, since we have a unique geometrical model; but we are aware that all our LOS intensities are overestimated as compared to the actual Goryaev model. In order to roughly compare the $L\alpha$ and $L\beta$ results with the streamer model we selected two lines of sight: one at $1.05 R_\odot$ and the other at $1.9 R_\odot$.

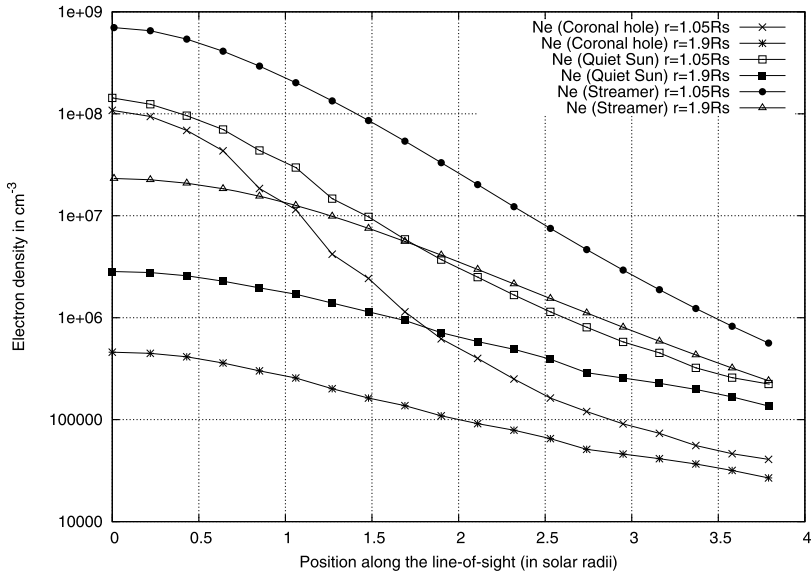


Figure 1 Electron densities for the quiet-Sun, coronal-hole, and streamer models at two altitudes: 1.05 and 1.9 R_{\odot} , along half of the LOS.

The initial density profile of the three models (quiet-Sun, coronal-hole, and streamer models) along the half of the LOS is shown in Figure 1.

We note that our streamer electron density (half) profiles along the LOS have roughly the same magnitudes and shapes as the streamer profile of Labrosse, Li, and Li (2006).

As far as the temperature profile is concerned, as mentioned above, we used the temperature variation with altitude of Allen (1977) for the quiet Sun. We took a constant temperature of 800,000 K (see David *et al.*, 1998) for the coronal-hole model and, as mentioned above, kept a constant temperature of 10^6 K for the streamer model (see Goryaev *et al.*, 2014).

3. Computed Profiles and Variation of the Integrated Intensities with the Altitude of the LOS

Since we assume no velocity field (neither radial nor along the LOS), we only compute half-profiles, which are shown in Figures 2 ($L\alpha$), 3 ($L\beta$), and 4 ($H\alpha$). Note that we limit ourselves to the presentation of the three lines, but more lines have been computed since we have a five-level atom.

It is important to stress that the $H\alpha$ (half) profiles in Figure 4 have been computed without any continuum absorption. This allows one to compare the integrated intensities in the three main lines on one hand (Figures 5 and 6) and, as far as the streamer is concerned, to compare with the $L\alpha$, $L\beta$ results of Labrosse, Li, and Li (2006), on the other hand. However, as shown in this section, the inclusion of absorption is critical for the $H\alpha$ line.

First, we note that for all models (Figures 5 and 6) the $L\beta$ intensity is an order of magnitude smaller than the $L\alpha$ intensity at $r = 1.05 R_{\odot}$, leading to a ratio (0.07) which is higher than the ratio of the incident intensities (between 0.011 and 0.014 according to Lemaire *et al.*, 2012). This ratio becomes 1.3×10^{-2} at $1.9 R_{\odot}$, a value equal to the ratio of the

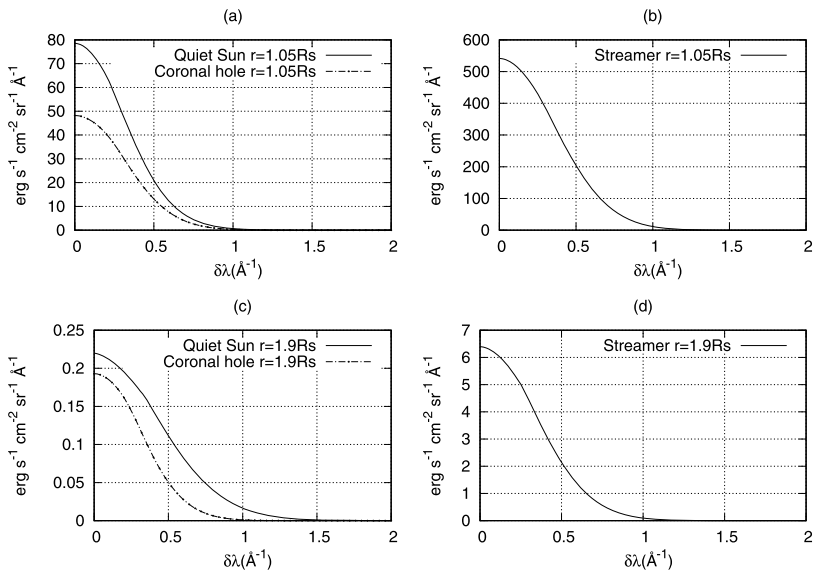


Figure 2 (a) and (b) Half profiles of the $L\alpha$ line for the LOS at $1.05 R_{\odot}$. (c) and (d) Half profiles of the $L\alpha$ line for the LOS at $1.9 R_{\odot}$. On the left column ((a) and (c)) the half-profiles for the quiet-Sun and coronal-hole models. On the right column ((b) and (d)) the half-profiles for the streamer model.

incident intensities and to be compared with the 2×10^{-3} observed value of Ciaravella *et al.* (2003) at a distance of $2.3 R_{\odot}$ in a pre-CME streamer (and a value slightly higher in the CME, or its “prominence core”, as stated by these authors). This can be interpreted as the result of the large (average) densities in our one-dimensional streamer model, which increase the collisional component of the $L\beta$ intensity and the excitation of level 3 through 1–2 and 2–3 absorption and spontaneous emission from level 3 to level 1.

Second, another interesting feature is the ratio between the $L\beta$ and $H\alpha$ integrated intensities which appears to be rather constant with the altitude and the model. Whatever the model and the altitude (see Figures 5 and 6), the value found is about eight which transforms into 1.2 when we compute the ratio of intensities in number of photons instead of energy intensities. We can compare this value with the ratio of spontaneous emission factors $[A_{ij}]$ in the $L\beta$ and $H\alpha$ lines (Heinzel, 2016, private communication). This is difficult because of the fact that the $L\beta$ line has three components and the $H\alpha$ line has eight components (Kramida *et al.*, 2015). In our computations, we adopted $A_{31} = 5.5 \times 10^7$ and $A_{32} = 4.4 \times 10^7$, which leads to $A_{31}/A_{32} = 1.25$, a value not very different from the ratio of the number of emitted photons. This is no surprise since the two lines share the same upper level and all emission processes other than spontaneous emission are negligible.

Third, our code can take into account the various continuum contributions (Thomson scattering, H^- , Rayleigh, *etc.*) but the only significant contribution comes from Thomson scattering, since the plasma is quite fully ionized. With Thomson opacity included (about 3×10^{-6}) the intensity in the wings of $H\alpha$ is notably increased (Figures 7, 8, and 9) and the profile is now in absorption. The relative absorption can easily be compared with the continuum within an order of magnitude. Even if the Thomson cross-section is about 11 orders of magnitude smaller than the $H\alpha$ absorption cross-section, we must take into account that the ratio of neutral (level 1) hydrogen to electron density populations is about $10^{-6} - 10^{-7}$ (see Section 5) or lower, as we shall see in Section 5, at the location of the impact param-

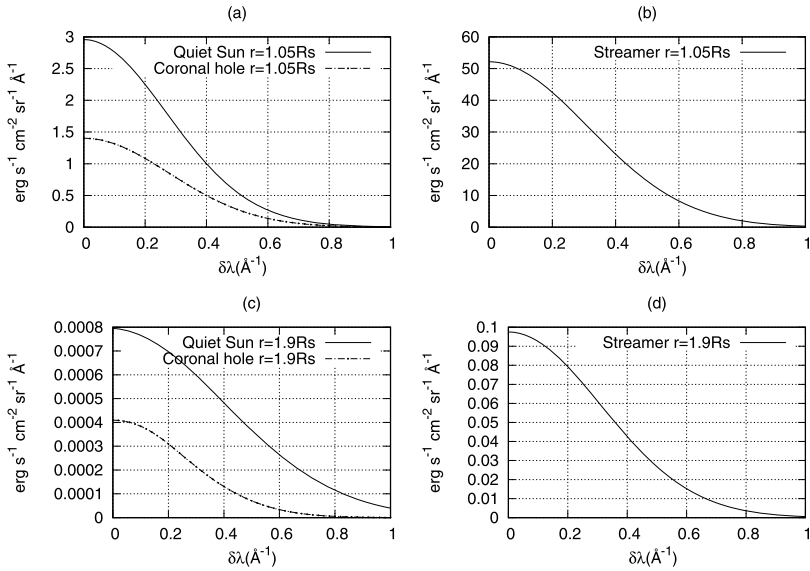


Figure 3 (a) and (b) Half profiles of the $L\beta$ line for the LOS at $1.05 R_{\odot}$. (c) and (d) Half-profiles of the $L\beta$ line for the LOS at $1.9 R_{\odot}$. On the left column ((a) and (c)) the half-profiles for the quiet-Sun and coronal-hole models. On the right column ((b) and (d)) the half-profiles for the streamer model.

ter (*i.e.* at the closest position to the Sun on the LOS) for Allen’s model (Allen, 1977) (see Figure 10). We also take into account that the ratio of level 2 to level 1 populations is less than 10^{-7} for the same model and at the same altitudes.

Consequently the $H\alpha$ contribution is about two orders of magnitude smaller than the Thomson scattering and it decreases with increasing altitude. The profile is in absorption (due to the fact that the $H\alpha$ incident profile is in absorption) and the depth of the depression is about 80 % of the local continuum. The width of the absorption line is about 2 \AA .

We do not present the comparison of $L\alpha$ and $L\beta$ profiles with and without continuum absorption because the continuum contribution is found to be negligible. This confirms why the measurement of the Thomson scattering at the $L\alpha$ wavelength with UVCS has been very difficult and consequently the Thomson scattering does not impede the purely $L\alpha$ scattering (Kohl *et al.*, 2007).

4. Comparison with Lyman Observations

As far as $L\alpha$ is concerned, we compare with profiles and intensities of Withbroe *et al.* (1982). These authors show the relative variation of $L\alpha$ with altitude (their Figure 2). They find a $L\alpha$ width ($1/e$ halfwidth) which decreases from about 0.75 to 0.58 \AA between 1.5 and $3.5 R_{\odot}$. At $1.9 R_{\odot}$, they find 0.7 \AA , to be compared with our 0.65 \AA (it should be recalled that their spectroscopic data are corrected for an instrumental width of 0.34 \AA).

As far as intensities are concerned, the Withbroe’s *et al.* values, when converted into cgs units, are higher than ours by about a factor three, at about all altitudes. This means that the ratio of intensities at 1.9 and $3.5 R_{\odot}$ is the same (about ten) for measured and computed values.

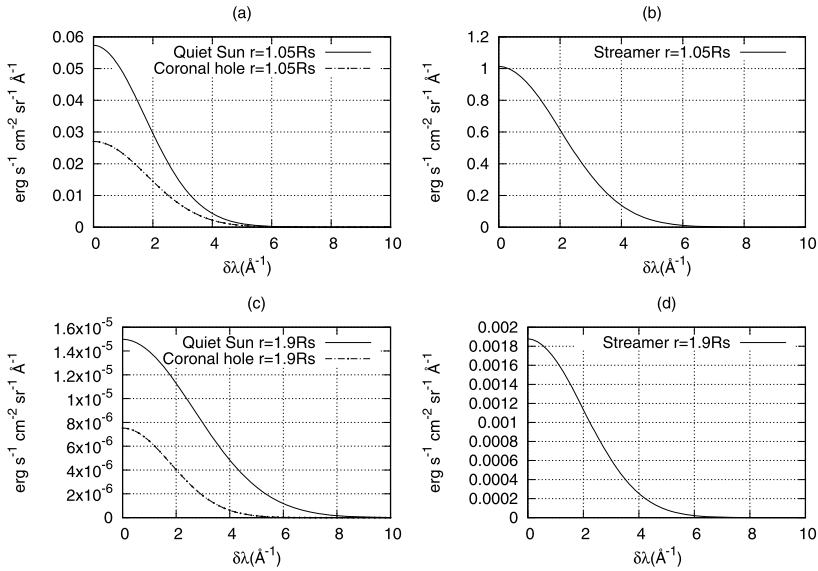


Figure 4 (a) and (b) Half profiles of the $H\alpha$ line for the LOS at $1.05 R_{\odot}$. (c) and (d) Half profiles of the $H\alpha$ line for the LOS at $1.9 R_{\odot}$. On the left column ((a) and (c)) the half profiles for the quiet-Sun and coronal-hole models. On the right column ((b) and (d)) the half profiles for the streamer model.

As far as coronal holes are concerned, a UVCS/SOHO intensity varying between 4×10^9 and 6×10^9 photons $\text{s}^{-1} \text{cm}^{-2} \text{sr}^{-1}$ is found by Bemporad, Matthaeus, and Poletto (2008) (see their Figure 2) from the center to the far edge of a polar coronal hole at an altitude of $2.14 R_{\odot}$. Once converted in $\text{erg s}^{-1} \text{cm}^{-2} \text{sr}^{-1}$, these values (0.06 and 0.096) are quite comparable with our value ($0.1 \text{ erg s}^{-1} \text{cm}^{-2} \text{sr}^{-1}$) at the same altitude.

We also compare our results with streamer observations. As far as profiles are concerned, Miralles *et al.* (1999) find a $1/e$ halfwidth varying from 0.75 \AA (their northern streamer) and 0.65 \AA (their southern streamer), at an altitude between 1.6 and $2.6 R_{\odot}$. We find (Figure 2) 0.5 \AA at $1.9 R_{\odot}$.

We also compare with Dolei, Spadaro, and Ventura (2015) who derived the H kinetic temperature (their Figure 11) from the $L\alpha$ halfwidth. Their values are higher than the one we adopted but the authors mentioned that their values are “higher than those determined by Spadaro *et al.* (2007) and Susino *et al.* (2008)”. As far as intensities are concerned, Miralles *et al.* (1999) find 0.8 to $1.3 \text{ erg s}^{-1} \text{cm}^{-2} \text{sr}^{-1}$ at $1.9 R_{\odot}$ (their Figure 2) and Dolei, Spadaro, and Ventura (2015) find 0.9 and $0.01 \text{ erg s}^{-1} \text{cm}^{-2} \text{sr}^{-1}$ at 1.9 and $5 R_{\odot}$, respectively. Our values are very close: 0.7 and $0.01 \text{ erg s}^{-1} \text{cm}^{-2} \text{sr}^{-1}$ at 1.9 and $5 R_{\odot}$, respectively.

5. Ionization Degree in the Low Corona

For the three models considered, we are able to compute exactly the variation of the ionization, defined here as n_e/n_{H_0} or n_e/n_1 where n_{H_0} is the neutral hydrogen density and n_1 is the fundamental level population (we do not include the He contribution to n_e). The values are in the expected range: for the quiet-Sun model, the ionization degree increases from 4×10^6 close to the surface to 2×10^7 between 1.5 and $2.5 R_{\odot}$. Then it slightly decreases to 1.4×10^7 at $5 R_{\odot}$. This behavior exactly matches the variation of temperature with altitude

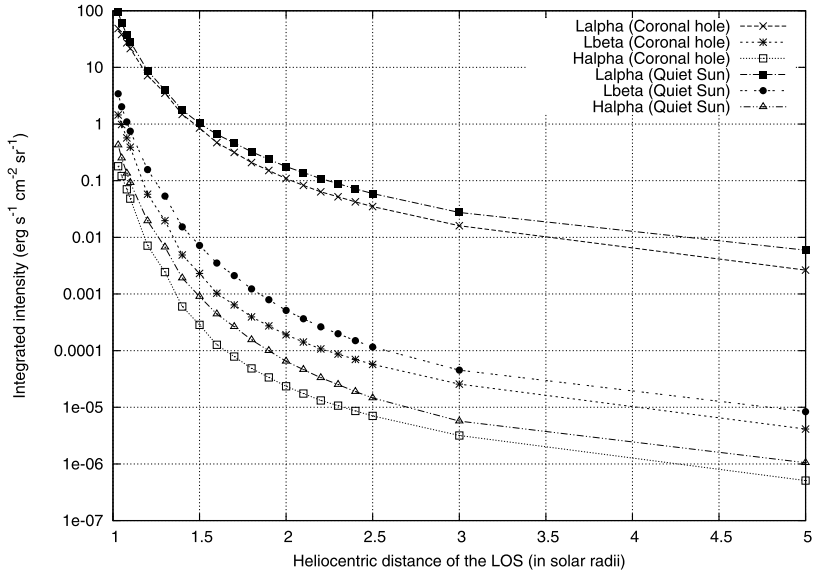


Figure 5 Variation of the integrated intensities of the $L\alpha$, $L\beta$, and $H\alpha$ lines [$\text{erg s}^{-1} \text{cm}^{-2} \text{sr}^{-1}$] with the position of the LOS (in solar radii) for the quiet-Sun and coronal-hole model where continuum absorption is omitted.

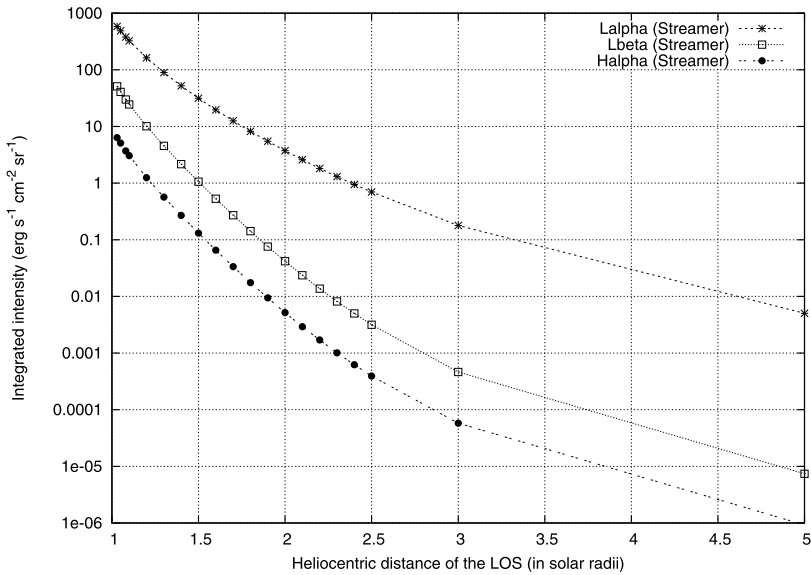


Figure 6 Variation of the integrated intensities of the $L\alpha$, $L\beta$, and $H\alpha$ lines [$\text{erg s}^{-1} \text{cm}^{-2} \text{sr}^{-1}$] with the position of the LOS (in solar radii) for the streamer model where continuum absorption is omitted.

(Figure 10): with increasing temperature, all factors implying ionization, especially the collisional terms, increase (see Cranmer *et al.*, 1999). The values imply a n_1/n_e ratio varying

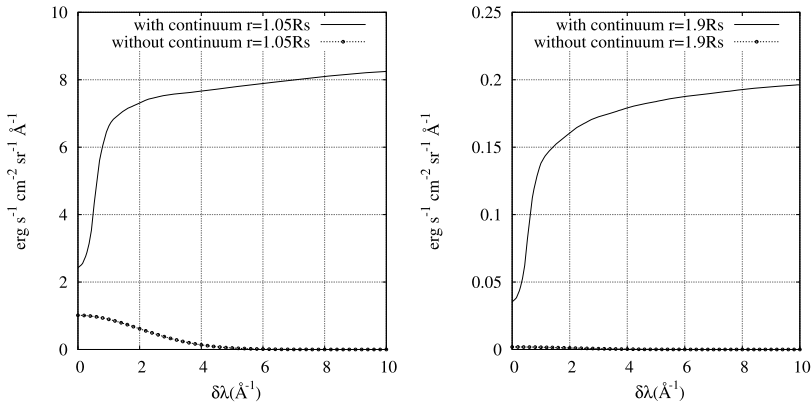


Figure 7 Comparison of H α half-profiles with and without continuum for the streamer model. Left: at $R = 1.05 R_{\odot}$. Right: at $1.9 R_{\odot}$.

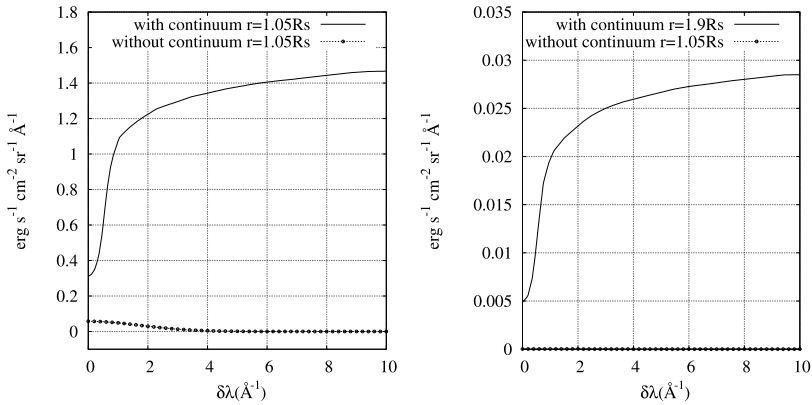


Figure 8 Comparison of H α half-profiles with and without continuum for the quiet-Sun model. Left: at $R = 1.05 R_{\odot}$. Right: at $1.9 R_{\odot}$.

from about 2.5×10^{-7} to 5×10^{-8} , which are lower, by an order of magnitude, than the values usually adopted in the corona (*e.g.* Gabriel, 1971). Note that Gabriel points out that his computation neglects photoionization from level 2. Here we stress that our computations include all hydrogen radiative terms. Note that the ionization degree is nearly constant for the coronal-hole (6×10^6) and streamer (8×10^6) models where the temperature is taken as constant (800,000 and 10^6 K, respectively).

6. Discussion

Let us note that since we have a five-level atom, we actually treat more transitions [$L\gamma$, H β , P α , H γ , P β , H δ , H ϵ] than the three presented above. Half profiles and integrated intensities of all these lines are available on the Multi Experiment Data and Operation Center (MEDOC) site https://idoc.ias.u-psud.fr/MEDOC/Radiative_transfer_codes/PROMCOR.

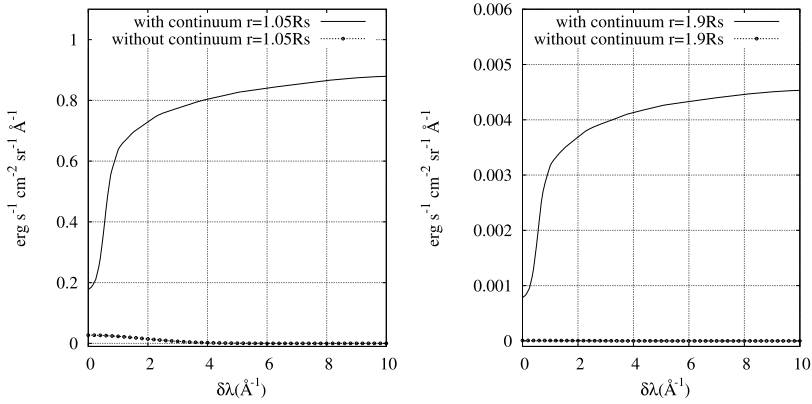


Figure 9 Comparison of $H\alpha$ half-profiles with and without continuum for the coronal-hole model. Left: at $R = 1.05 R_{\odot}$. Right: at $1.9 R_{\odot}$.

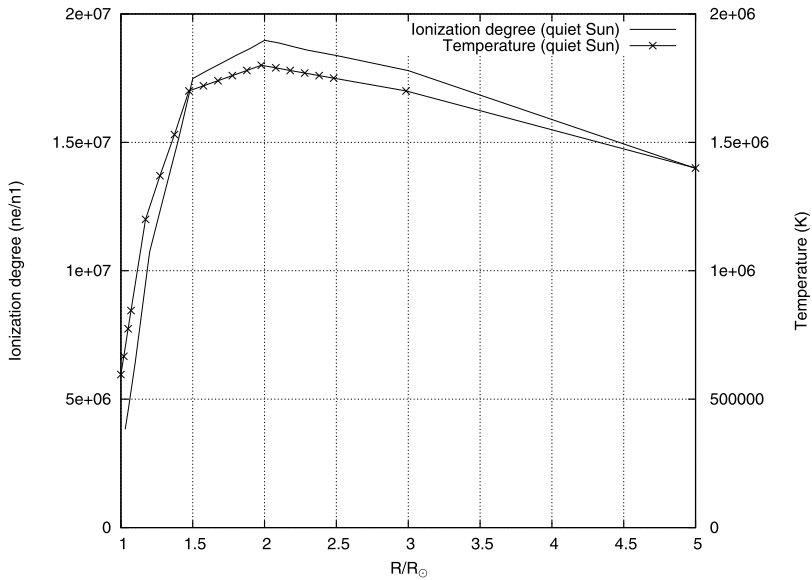


Figure 10 Variation of the ionization degree (as defined by the ratio of electron to neutral hydrogen densities) and the temperature [K] with altitude (in solar radii) for the quiet-Sun model of Allen (1977). We indicate the ionization degree with a solid line and the temperature with x signs.

We now raise the issue of the visibility of the hydrogen lines in the corona and in particular the polarimetry, since, as mentioned in many proposals and roadmaps (see, *e.g.*, Schrijver *et al.*, 2015) the measurement of the coronal magnetic field, is now a major objective in solar physics.

First, as shown in Section 4, we are not surprised as far as the $L\alpha$ line is concerned, since the UVCS measurements (Figure 11) at a distance as low as $1.5 R_{\odot}$ are close to our computations for our streamer model (see Figure 6). The $L\alpha$ variation of Figure 6 shows that at $2.5 R_{\odot}$ ($1.5 R_{\odot}$ above the surface) the $L\alpha$ intensity is about 1.4×10^{-5} the disk intensity.

This altitude is the maximum altitude where linear polarization measurements can provide useful information as regards the coronal magnetic field through the Hanle effect (Derouich *et al.*, 2010). This value seems to be compatible with the scattering performances of the proposed instrumentation (*e.g.* Vial *et al.*, 2007). However, it is clear that the coronal intensity is about a magnitude lower in a quiet corona and still lower in coronal holes (Figure 5) which means that measurements will be challenging at those locations.

Second, as for $L\beta$, in our streamer model the intensity variation with distance compares relatively well to the results of Labrosse, Li, and Li (2006) in terms of number of photons. According to Giordano *et al.* (2013), the $L\beta$ intensity is $0.03 \text{ erg s}^{-1} \text{ cm}^{-2} \text{ sr}^{-1}$ at $1.9 R_{\odot}$ where we find 0.09 (note that the $L\alpha$ values are closer: 8 for our computations and 6.4 for Giordano *et al.*, 2013 at $1.9 R_{\odot}$). The ratio $L\beta/L\alpha$ is about 10^{-3} as in Labrosse, Li, and Li (2006) at $3 R_{\odot}$, but it is about 10^{-1} instead of 10^{-2} in Labrosse, Li, and Li (2006) for $1 R_{\odot}$. With the quiet-Sun (Allen) model, the $L\beta/L\alpha$ ratio is lower than 10^{-1} at $1 R_{\odot}$ and 2×10^{-3} at $2.5 R_{\odot}$, which means that polarization measurements in the $L\beta$ line (Peter *et al.*, 2012) will face serious difficulties because of the low signal-to-noise ratio.

Third, as far as the $H\alpha$ intensity is concerned, Figures 5 and 6 provide useful information on the proper line emission (lower than the $L\beta$ line by a factor eight). But in order to evaluate the feasibility of $H\alpha$ measurements in the corona and even possibly polarimetric ones, one definitely needs to take into account the continuum (Thomson) absorption and scattering. From Figures 7, 8, and 9, one can compute the variation of the integrated intensity with the width of the integration band (or bandpass).

At $1.05 R_{\odot}$, over a 2 \AA bandpass, we find $8.6 \text{ erg s}^{-1} \text{ cm}^{-2} \text{ sr}^{-1}$ for the streamer model and $0.16 \text{ erg s}^{-1} \text{ cm}^{-2} \text{ sr}^{-1}$ at $1.9 R_{\odot}$. For the quiet Sun, the values are still much lower (1.3 and $0.02 \text{ erg s}^{-1} \text{ cm}^{-2} \text{ sr}^{-1}$, respectively; see Table 1).

Although these values are very low, the contrast of intensities between the streamer and the equatorial quiet Sun is of the order of seven. This means that with the technique of background subtraction currently used in coronagraphic data, it is possible to access $H\alpha$ in the coronal extension of active regions, provided that the bandpass is equal to or less than 2 \AA .

As far as coronal holes are concerned, the $H\alpha$ intensity (slightly dependent on the temperature) is 0.8 at $1.05 R_{\odot}$ and $3.7 \times 10^{-3} \text{ erg s}^{-1} \text{ cm}^{-2} \text{ sr}^{-1}$ at $1.9 R_{\odot}$. The contrast of the $H\alpha$ coronal hole (ratio to the quiet Sun) is 0.6 at $1.05 R_{\odot}$ and 0.19 at $1.9 R_{\odot}$. These numbers will actually be higher because of the LOS contamination; this leaves a small hope for detection in $H\alpha$ of out-of-the limb coronal holes.

The possibility of performing polarimetric measurements in $H\alpha$ has been discussed by Kim *et al.* (2013a) who included the effect of instrumental stray light. Our computations show that the $H\alpha$ polarimetry in the corona could be envisaged above active regions with an instrumentation with a large aperture. However, the complexity of the line and its separation between polarizable and non-polarizable states (Dubau, 2015, private communication) make the interpretation complex, as noted by Leenaarts, Carlsson, and Rouppe van der Voort (2012) for the chromosphere.

Finally the $H\alpha$ results are summarized in Table 1.

7. Conclusions

Since we have the tools for computing exactly the ionization degree and the hydrogen-line emission in the corona, we envisage further improvements that will allow using more complex and realistic models.

Table 1 Integrated intensity [$\text{erg s}^{-1} \text{cm}^{-2} \text{sr}^{-1}$] of the $\text{H}\alpha$ line as a function of the bandpass [\AA], for the quiet-Sun, coronal-hole, and streamer models at positions 1.05 and 1.9 R_{\odot} of the LOS.

Bandpass \AA	Quiet Sun 1.05 R_{\odot}	Quiet Sun 1.9 R_{\odot}	Coronal hole 1.05 R_{\odot}	Coronal hole 1.9 R_{\odot}	Streamer 1.05 R_{\odot}	Streamer 1.9 R_{\odot}
1	3.97×10^{-1}	6.7×10^{-3}	2.31×10^{-1}	1.06×10^{-3}	2.91	4.72×10^{-2}
1.5	7.87×10^{-1}	1.37×10^{-2}	4.61×10^{-1}	2.19×10^{-3}	5.43	9.65×10^{-2}
2	1.29	2.3×10^{-2}	7.60×10^{-1}	3.67×10^{-3}	8.57	1.61×10^{-1}
3	2.42	4.4×10^{-2}	1.43	7.01×10^{-3}	15.5	3.07×10^{-1}
4	3.61	6.65×10^{-2}	2.14	1.06×10^{-2}	22.7	4.63×10^{-1}
5	4.86	9.03×10^{-2}	2.89	1.44×10^{-2}	30.1	6.27×10^{-1}

First, we plan to include velocity fields which implies to compute a dilution factor taking into account the effect of velocities on the limb darkening or brightening of the incident radiation (the so-called ‘‘Doppler dimming effect’’; see, *e.g.*, Hyder and Lites, 1970). We also plan to take into account non-axisymmetric illumination due to, *e.g.*, the proximity of an active region. Moreover, in order to compute exactly the electron population, we plan to include He in the ionization balance. Finally, we could also include a scattering dependent on the angle between incident and emergent radiations. We can also think of a modeling, where proton and electron temperatures are different (Marsch *et al.*, 1999).

Second, we plan to use 2D or 3D coronal models (whether MHD or empirical) with full consistency between the various thermodynamic parameters and complex geometries.

The combination of better tools for the computation of the ionization and the emission in the corona, along with realistic thermodynamic models of the corona, will allow for the interpretation of observations from future missions such as *Solar Orbiter*.

Acknowledgements This paper is dedicated to Lola Salines, who was murdered in Paris on 13 November 2015. The authors thank Pierre Gouttebroze, Iraida Kim, and Serge Koutchmy for useful comments. They cordially thank the referee for comments which helped to improve the paper and clarify its aims.

Disclosure of Potential Conflict of Interest The authors declare that they have no conflicts of interest.

Appendix

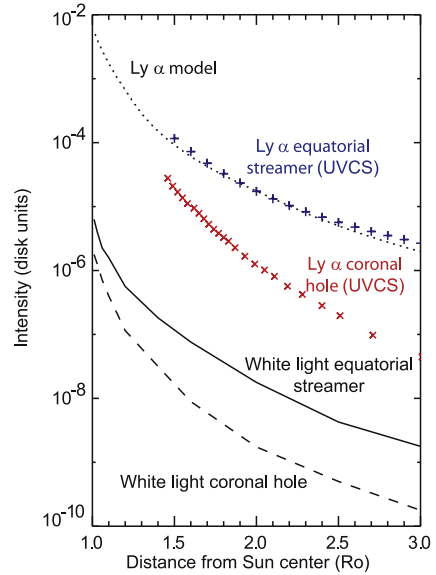
This appendix is focused on a simple derivation of the $\text{H}\alpha$ coronal emission from the (measured) $\text{L}\alpha$ emission.

We proceed in two steps. First, we only consider a three-level hydrogen atom which involves the $\text{L}\alpha$, $\text{L}\beta$, and $\text{H}\alpha$ lines and we exclude any polarization analysis. Then, we take into account the incident and scattered continua (essentially Thomson scattering) that we superimpose on the hydrogen emission in order to predict the actual emerging $\text{H}\alpha$ intensity.

We assume that the emission in these three lines results from only the process of resonance scattering. This means that level 3 is populated through two processes: $\text{L}\beta$ absorption from level 1 and $\text{H}\alpha$ absorption from level 2. We also assume, as a first step, that the $\text{H}\alpha$ emission results only from the $\text{H}\alpha$ absorption and we neglect $3 \rightarrow 2 \rightarrow 1$ cascade from $\text{L}\beta$ absorption. Consequently, we can compare the emissions in $\text{L}\alpha$ and $\text{H}\alpha$ which share the level 2.

Since we have some values of the $\text{L}\alpha$ intensity in the corona, we hope to be able to derive $\text{H}\alpha$ intensities. We can obtain a synthetic view of the variation of the $\text{L}\alpha$ intensity *versus*

Figure 11 Variation of the $L\alpha$ and white-light intensities (normalized to the disk-averaged intensities) with the distance to Sun center for two coronal regions: coronal hole and equatorial streamer. The $L\alpha$ data are from UVCS, the white-light data from Koutchmy (2006, private communication). Reproduced from Vial *et al.* (2007)



altitude in the corona for two types of structures: a streamer and a coronal hole (Figure 11 taken from Vial *et al.*, 2007).

The $H\alpha$ absorbed and emitted intensity is

$$I^{H\alpha}(r_0) = B_{23} \frac{h\nu^{H\alpha}}{4\pi} \int_{-\infty}^{+\infty} n_2(s) \int_0^{+\infty} \int_{\Omega} I_{\text{inc}}^{H\alpha}(v, \omega) \frac{d\omega}{4\pi} \phi^{H\alpha}(v, s) dv ds. \quad (1)$$

The $L\alpha$ absorbed intensity is

$$I^{L\alpha}(r_0) = B_{12} \frac{h\nu^{L\alpha}}{4\pi} \int_{-\infty}^{+\infty} n_1(s) \int_0^{+\infty} \int_{\Omega} I_{\text{inc}}^{L\alpha}(v, \omega) \frac{d\omega}{4\pi} \phi^{L\alpha}(v, s) dv ds. \quad (2)$$

The $L\alpha$ emitted intensity is

$$I^{L\alpha}(r_0) = A_{21} \frac{h\nu^{L\alpha}}{4\pi} \int_{-\infty}^{+\infty} n_2(s) ds \int_0^{+\infty} \phi(\lambda) d\lambda \quad (3)$$

where $\phi(v, s)$ is the absorption profile at position s , where s is the distance of point M along the ray taken from the impact point P (at altitude r_0).

$I_{\text{inc}}(v, \omega)$ (or $I_{\text{inc}}(\lambda, \omega)$) is the incident radiation at position $M(s)$, depending on the frequency [ν] (or wavelength [λ]) and solid angle [ω].

With the transformation $ds = \frac{r dr}{\sqrt{r^2 - r_0^2}}$, Equations (1), (2), and (3) become Volterra integral equations of the first kind. But the kernels are complex and include singularities. Consequently, we proceed with important simplifications where the quantity $\int I_{\text{inc}}(\lambda, \omega) \frac{d\omega}{4\pi} d\lambda \phi(\lambda)$ (or $\int I_{\text{inc}}(v, \omega) \frac{d\omega}{4\pi} dv \phi(v)$) is replaced in Equations (1) and (2) by $\langle I_{\text{emitted}} \rangle \times w(r_0) \times \text{FWHM}$, where $w(r_0) = 0.5(1 - \sqrt{1 - (\frac{R}{r_0})^2})$ is the dilution factor taken at r_0 . Equation (1) becomes

$$I^{H\alpha}(r_0) = B_{23} \frac{h\nu^{H\alpha}}{4\pi} \int_{-\infty}^{+\infty} n_2(s) ds \langle I_{\text{emitted}}^{H\alpha} \rangle w(r_0) \text{FWHM}_{H\alpha}$$

where $\langle I_{\text{emitted}} \rangle$ is the chromospheric (incident) integrated emission that, when possible, we replace by the product of the half-intensity by the full width at half maximum (FWHM).

We have considered that $\phi^{H\alpha}(v, s)$ or $\phi^{H\alpha}(\lambda, s)$ depends (weakly) on temperature which is about 10^6 K. Then the Doppler width is $\Delta\lambda_D^{H\alpha} \approx 2.8 \text{ \AA}$ and the FWHM = $2\sqrt{\log_e 2} \Delta\lambda_D = 4.7 \text{ \AA}$. We also replace $\int n_2 ds$ by $n_2(r_0)\Delta s$, where Δs is the LOS distance over which n_2 is significant.

The incident radiation is taken from David (1961) for $H\alpha$ and from Makarova and Kharitonov (1969) for the nearby continuum. We take an average value of 60 % of the continuum over a FWHM of 4.7 \AA . Equation (1) becomes

$$I^{H\alpha}(r_0) = B_{23} \frac{h\nu^{H\alpha}}{4\pi} n_2(r_0) \Delta s \langle I_{\text{emitted}}^{H\alpha} \rangle w(r_0) \text{FWHM}(H\alpha). \quad (4)$$

Similarly, Equation (2) becomes

$$I^{L\alpha}(r_0) = B_{12} \frac{h\nu^{L\alpha}}{4\pi} n_1(r_0) \Delta s \langle I_{\text{emitted}}^{L\alpha} \rangle w(r_0) \text{FWHM}(L\alpha). \quad (5)$$

Note that we take the same Δs along which the densities (n_1, n_2, \dots) are significant. This is not different from computing the emission at position $P(r_0)$. Then, Equation (3) becomes

$$I^{L\alpha}(r_0) = A_{21} \frac{h\nu^{L\alpha}}{4\pi} n_2(r_0) \Delta s \text{FWHM}(L\alpha). \quad (6)$$

The ratio between Equations (4) and (6) gives

$$\frac{I^{H\alpha}(r_0)}{I^{L\alpha}(r_0)} = \frac{B_{23}}{A_{21}} \frac{\nu^{H\alpha}}{\nu^{L\alpha}} \langle I_{\text{emitted}}^{H\alpha} \rangle w(r_0) \frac{\text{FWHM}(H\alpha)}{\text{FWHM}(L\alpha)}. \quad (7)$$

The $L\alpha$ emission is taken from Figure 11 at 1.05 and 1.9 R_\odot . With the respective values of $w(r)$ (0.35 at 1.05 R_\odot and 0.075 at 1.9 R_\odot), the ratio $\frac{\text{FWHM}(H\alpha)}{\text{FWHM}(L\alpha)}$ taken at 10^6 K as 9.3, we find, for a 4.7 \AA bandpass, 107.5 and 0.23 $\text{erg s}^{-1} \text{cm}^{-2} \text{sr}^{-1}$ at 1.05 and 1.9 R_\odot , respectively. Table 1 provides exact values which are about 3 times weaker at both altitudes. This agreement, which is well within an order of magnitude, is rather satisfactory when we take into account the many assumptions made in our analytical computation on one hand, and our use of coronal models that may well not represent reality, on the other hand. However, this computation has the advantage of providing a simple rule (Equation (7)) for deriving the $H\alpha$ intensity whenever and wherever the $L\alpha$ intensity is measured.

References

- Allen, K.W.: 1977, *Astrophysical Quantities*, 3rd edn., London. [ADS](#).
- Antonucci, E., Fineschi, S., Naletto, G., Romoli, M., Spadaro, D., Nicolini, G., Nicolosi, P., Abbo, L., Andretta, V., Bemporad, A., Auchère, F., Berlicki, A., Bruno, R., Capobianco, G., Ciaravella, A., Crescenzo, G., Da Deppo, V., D'Amicis, R., Focardi, M., Frassetto, F., Heinzel, P., Lamy, P.L., Landini, F., Massone, G., Malvezzi, M.A., Moses, J.D., Pancrazzi, M., Pelizzo, M.-G., Poletto, L., Schühle, U.H., Solanki, S.K., Telloni, D., Teriaca, L., Uslenghi, M.: 2012, Multi Element Telescope for Imaging and Spectroscopy (METIS) coronagraph for the Solar Orbiter mission. In: *Space Telescopes and Instrumentation 2012: Ultraviolet to Gamma Ray*, *Proc. SPIE* **8443**, 844309. [DOI](#). [ADS](#).
- Anzer, U., Heinzel, P.: 1999, The energy balance in solar prominences. *Astron. Astrophys.* **349**, 974. [ADS](#).
- Auchère, F.: 2005, Effect of the H I Ly α chromospheric flux anisotropy on the total intensity of the resonantly scattered coronal radiation. *Astrophys. J.* **622**, 737. [DOI](#). [ADS](#).
- Bemporad, A., Matthaeus, W.H., Poletto, G.: 2008, Low-frequency Ly α power spectra observed by UVCS in a polar coronal hole. *Astrophys. J. Lett.* **677**, L137. [DOI](#). [ADS](#).
- Bommier, V., Sahal-Brechot, S.: 1982, The Hanle effect of the coronal L-alpha line of hydrogen-theoretical investigation. *Solar Phys.* **78**, 157. [DOI](#). [ADS](#).
- Bommier, V., Sahal-Brechot, S., Leroy, J.L.: 1981, Determination of the complete vector magnetic field in solar prominences, using the Hanle effect. *Astron. Astrophys.* **100**, 231. [ADS](#).

- Ciaravella, A., Raymond, J.C., van Ballegoijen, A., Strachan, L., Vourlidis, A., Li, J., Chen, J., Panasyuk, A.: 2003, Physical parameters of the 2000 February 11 coronal mass ejection: ultraviolet spectra versus white-light images. *Astrophys. J.* **597**, 1118. DOI. ADS.
- Cranmer, S.R., Kohl, J.L., Noci, G., Antonucci, E., Tondello, G., Huber, M.C.E., Strachan, L., Panasyuk, A.V., Gardner, L.D., Romoli, M., Fineschi, S., Dobrzycka, D., Raymond, J.C., Nicolosi, P., Siegmund, O.H.W., Spadaro, D., Benna, C., Ciaravella, A., Giordano, S., Habbal, S.R., Karovska, M., Li, X., Martin, R., Michels, J.G., Modigliani, A., Naletto, G., O'Neal, R.H., Pernechele, C., Poletto, G., Smith, P.L., Suleiman, R.M.: 1999, An empirical model of a polar coronal hole at solar minimum. *Astrophys. J.* **511**, 481. DOI. ADS.
- David, C., Gabriel, A.H., Bely-Dubau, F., Fludra, A., Lemaire, P., Wilhelm, K.: 1998, Measurement of the electron temperature gradient in a solar coronal hole. *Astron. Astrophys.* **336**, L90. ADS.
- David, K.-H.: 1961, Die Mitte-Rand Variation der Balmerlinien $H\alpha$ - $H\delta$ auf der Sonnenscheibe. Mit 9 Textabbildungen. *Z. Astrophys.* **53**, 37. ADS.
- Derouchi, M., Auchère, F., Vial, J.C., Zhang, M.: 2010, Hanle signatures of the coronal magnetic field in the linear polarization of the hydrogen $L\alpha$ line. *Astron. Astrophys.* **511**, A7. DOI. ADS.
- Dolei, S., Spadaro, D., Ventura, R.: 2015, Visible light and ultraviolet observations of coronal structures: physical properties of an equatorial streamer and modelling of the F corona. *Astron. Astrophys.* **577**, A34. DOI. ADS.
- Dolei, S., Romano, P., Spadaro, D., Ventura, R.: 2014, Stereoscopic observations of the effects of a halo CME on the solar coronal structure. *Astron. Astrophys.* **567**, A9. DOI. ADS.
- Gabriel, A.H.: 1971, Measurements on the Lyman alpha corona. *Solar Phys.* **21**, 392. DOI. ADS.
- Giordano, S., Ciaravella, A., Raymond, J.C., Ko, Y.-K., Suleiman, R.: 2013, UVCS/SOHO catalog of coronal mass ejections from 1996 to 2005: spectroscopic properties. *J. Geophys. Res.* **118**, 967. DOI. ADS.
- Goryaev, F., Slemzin, V., Vainshtein, L., Williams, D.R.: 2014, Study of extreme-ultraviolet emission and properties of a coronal streamer from PROBA2/SWAP, Hinode/EIS and Mauna Loa Mk4 observations. *Astrophys. J.* **781**, 100. DOI. ADS.
- Gouttebroze, P., Heinzel, P., Vial, J.C.: 1993, The hydrogen spectrum of model prominences. *Astron. Astrophys. Suppl.* **99**, 513. ADS.
- Gunár, S.: 2014, Modelling of quiescent prominence fine structures. In: Schmieder, B., Malherbe, J.-M., Wu, S.T. (eds.) *Nature of Prominences and Their Role in Space Weather*, IAU Symp. **300**, 59. DOI. ADS.
- Hassler, D.M., Strachan, L., Gardner, L.D., Kohl, J.L., Guhathakurta, M., Fisher, R.R., Strong, K.: 1994, Ly-alpha and white light observations of a CME during the Spartan 201-1 mission. In: Hunt, J.J. (ed.) *Solar Dynamic Phenomena and Solar Wind Consequences, the Third SOHO Workshop*, SP-373, ESA, 363. ADS.
- Heasley, J.N., Mihalas, D.: 1976, Structure and spectrum of quiescent prominences – energy balance and hydrogen spectrum. *Astrophys. J.* **205**, 273. DOI. ADS.
- Heinzel, P.: 2015, Radiative transfer in Solar prominences. In: Vial, J.-C., Engvold, O. (eds.) *Solar Prominences*, *Astrophys. Space Scien. Lib.* **415**, 103. DOI. ADS.
- Heinzel, P., Anzer, U., Gunár, S.: 2005, Prominence fine structures in a magnetic equilibrium. II. A grid of two-dimensional models. *Astron. Astrophys.* **442**, 331. DOI. ADS.
- Hyder, C.L., Lites, B.W.: 1970, $H\alpha$ Doppler brightening and Lyman- α Doppler dimming in moving $H\alpha$ prominences. *Solar Phys.* **14**, 147. DOI. ADS.
- Kim, I.S., Alexeeva, I.V., Bugaenko, O.I., Popov, V.V., Suyunova, E.Z.: 2013a, Near-Limb Zeeman and Hanle diagnostics. *Solar Phys.* **288**, 651. DOI. ADS.
- Kim, I.S., Popov, V.V., Lisin, D.V., Osokin, A.P.: 2013b, Observations of neutral hydrogen in the corona. *Geomagn. Aeron.* **53**, 901. DOI. ADS.
- Kohl, J.L., Gardner, L.D., Strachan, L., Fisher, R., Guhathakurta, M.: 1995, SPARTAN 201 coronal spectroscopy during the polar passes of ULYSSES. *Space Sci. Rev.* **72**, 29. DOI. ADS.
- Kohl, J.L., Panasyuk, A., Cranmer, S.R., Gardner, L.D., Raymond, J.C.: 2007, Measurements of coronal proton velocity distributions. *AGU Abs.*, A298. ADS.
- Koutchmy, S., Belmehdi, M., Coulter, R.L., Demoulin, P., Gaizauskas, V., MacQueen, R.M., Monnet, G., Mouette, J., Noens, J.C., November, L.J.: 1994, CFHT eclipse observation of the very fine-scale solar corona. *Astron. Astrophys.* **281**, 249. ADS.
- Kramida, A., Ralchenko, Y., Reader, J., NIST ASD Team (2015): 2015, Atomic Spectra Database (version 5.3), physics.nist.gov/asd. National Institute of Standards and Technology, Gaithersburg, MD.
- Labrosse, N.: 2015, Derivation of the major properties of prominences using NLTE modelling. In: Vial, J.-C., Engvold, O. (eds.) *Solar Prominences*, *Astrophys. Space Scien. Lib.* **415**, 131. DOI. ADS.
- Labrosse, N., Li, X., Li, B.: 2006, On the Lyman α and β lines in solar coronal streamers. *Astron. Astrophys.* **455**, 719. DOI. ADS.

- Labrosse, N., Heinzel, P., Vial, J.-C., Kucera, T., Parenti, S., Gunár, S., Schmieder, B., Kilper, G.: 2010, Physics of Solar prominences: I-spectral diagnostics and non-LTE modelling. *Space Sci. Rev.* **151**, 243. DOI. ADS.
- Leenaarts, J., Carlsson, M., Rouppe van der Voort, L.: 2012, The formation of the H α line in the solar chromosphere. *Astrophys. J.* **749**, 136. DOI. ADS.
- Lemaire, P., Vial, J.-C., Curdt, W., Schühle, U., Woods, T.N.: 2012, The solar hydrogen Lyman α to Lyman β line ratio. *Astron. Astrophys.* **542**, L25. DOI. ADS.
- Leroy, J.-L.: 1981, Simultaneous measurement of the polarization in H-alpha and D3 prominence emissions. *Solar Phys.* **71**, 285. DOI. ADS.
- Li, B., Li, X., Labrosse, N.: 2006, A global 2.5-dimensional three fluid solar wind model with alpha particles. *J. Geophys. Res.* **111**, A08106. DOI. ADS.
- Lin, H., Penn, M.J., Tomczyk, S.: 2000, A new precise measurement of the coronal magnetic field strength. *Astrophys. J. Lett.* **541**, L83. DOI. ADS.
- Maccari, L., Noci, G., Modigliani, A., Romoli, M., Fineschi, S., Kohl, J.L.: 1999, Ly- α observation of a coronal streamer with UVCS/SOHO. *Space Sci. Rev.* **87**, 265. DOI. ADS.
- Makarova, E.A., Kharitonov, A.V.: 1969, Mean absolute energy distribution in the solar spectrum from 1800 Å to 4 mm, and the solar constant *Soviet Astron.* **12**, 599. ADS.
- Marsch, E., Tu, C.-Y., Heinzel, P., Wilhelm, K., Curdt, W.: 1999, Proton and hydrogen temperatures at the base of the solar polar corona. *Astron. Astrophys.* **347**, 676. ADS.
- Mierla, M., Chifu, I., Inhester, B., Rodriguez, L., Zhukov, A.: 2011, Low polarised emission from the core of coronal mass ejections. *Astron. Astrophys.* **530**, L1. DOI. ADS.
- Miralles, M.P., Strachan, L., Gardner, L.D., Dobryzcka, D., Ko, Y.-K., Michels, J., Panasyuk, A., Suleiman, R., Kohl, J.L.: 1999, Streamer HI Ly- α line profiles during the Spartan 201-05/SOHO co-ordinated observations. In: Wilson, A., et al. (eds.) *Magnetic Fields and Solar Processes*, **SP-448**, ESA, 1193. ADS.
- Noci, G., Kohl, J.L., Withbroe, G.L.: 1987, Solar wind diagnostics from Doppler-enhanced scattering. *Astrophys. J.* **315**, 706. DOI. ADS.
- Peter, H., Abbo, L., Andretta, V., Auchère, F., Bemporad, A., Berrilli, F., Bommier, V., Braukhane, A., Casini, R., Curdt, W., Davila, J., Dittus, H., Fineschi, S., Fludra, A., Gandorfer, A., Griffin, D., Inhester, B., Lagg, A., Degl'Innocenti, E.L., Maiwald, V., Sainz, R.M., Pillet, V.M., Matthews, S., Moses, D., Parenti, S., Pietarila, A., Quantius, D., Raouafi, N.-E., Raymond, J., Rochus, P., Romberg, O., Schlöterter, M., Schühle, U., Solanki, S., Spadaro, D., Teriaca, L., Tomczyk, S., Bueno, J.T., Vial, J.-C.: 2012, Solar magnetism eXplorer (SolmeX). Exploring the magnetic field in the upper atmosphere of our closest star. *Exp. Astron.* **33**, 271. DOI. ADS.
- Poland, A.I., Munro, R.H.: 1976, Interpretation of broad-band polarimetry of solar coronal transients – importance of H-alpha emission. *Astrophys. J.* **209**, 927. DOI. ADS.
- Raymond, J.C., Kohl, J.L., Noci, G., Antonucci, E., Tondello, G., Huber, M.C.E., Gardner, L.D., Nicolosi, P., Fineschi, S., Romoli, M., Spadaro, D., Siegmund, O.H.W., Benna, C., Ciaravella, A., Cranmer, S., Giordano, S., Karovska, M., Martin, R., Michels, J., Modigliani, A., Naletto, G., Panasyuk, A., Pernechele, C., Poletto, G., Smith, P.L., Suleiman, R.M., Strachan, L.: 1997, Composition of coronal streamers from the SOHO ultraviolet coronagraph spectrometer. *Solar Phys.* **175**, 645. DOI. ADS.
- Schrijver, C.J., Kauristie, K., Aylward, A.D., Denardini, C.M., Gibson, S.E., Glover, A., Gopalswamy, N., Grande, M., Hapgood, M., Heynderickx, D., Jakowski, N., Kalegaev, V.V., Lapenta, G., Linker, J.A., Liu, S., Mandrini, C.H., Mann, I.R., Nagatsuma, T., Nandy, D., Obara, T., Paul O'Brien, T., Onsager, T., Opgenoorth, H.J., Terkildsen, M., Valladares, C.E., Vilmer, N.: 2015, Understanding space weather to shield society: a global road map for 2015–2025 commissioned by COSPAR and ILWS. *Adv. Space Res.* **55**, 2745. DOI. ADS.
- Spadaro, D., Susino, R., Ventura, R., Vourlidis, A., Landi, E.: 2007, Physical parameters of a mid-latitude streamer during the declining phase of the solar cycle. *Astron. Astrophys.* **475**, 707. DOI. ADS.
- Susino, R., Ventura, R., Spadaro, D., Vourlidis, A., Landi, E.: 2008, Physical parameters along the boundaries of a mid-latitude streamer and in its adjacent regions. *Astron. Astrophys.* **488**, 303. DOI. ADS.
- Tomczyk, S., Card, G.L., Darnell, T., Elmore, D.F., Lull, R., Nelson, P.G., Streaender, K.V., Burkpile, J., Casini, R., Judge, P.G.: 2008, An instrument to measure coronal emission line polarization. *Solar Phys.* **247**, 411. DOI. ADS.
- Vial, J.C.: 1970, Intensity distribution in the LYMAN- α line at the solar limb. In: Muller, R., Houziaux, L., Butler, H.E. (eds.) *Ultraviolet Stellar Spectra and Related Ground-Based Observations*, *IAU Symp.* **36**, 260. ADS.
- Vial, J.-C., Koutchmy, S., Monnet, G., Sovka, J., Clark, C., Salmon, D., Purves, N., Sydserff, P., Coulter, R., November, L.: 1992, Evidence of plasmoid ejection in the corona from 1991 eclipse observations with the Canada–France–Hawaii telescope. In: Dame, L., Guyenne, T.-D. (eds.), **SP-344**, ESA, 87. ADS.

-
- Vial, J.-C., Auchère, F., Chang, J., Fang, C., Gan, W.Q., Klein, K.-L., Prado, J.-Y., Trottet, G., Wang, C., Yan, Y.H.: 2007, SMESE: a SMall explorer for solar eruptions. *Adv. Space Res.* **40**, 1787. [DOI](#). [ADS](#).
- Withbroe, G.L., Kohl, J.L., Weiser, H., Munro, R.H.: 1982, Probing the solar wind acceleration region using spectroscopic techniques. *Space Sci. Rev.* **33**, 17. [DOI](#). [ADS](#).
- Zangrilli, L., Nicolosi, P., Poletto, G., Noci, G., Romoli, M., Kohl, J.L.: 1999, Latitudinal properties of the Lyman alpha and O VI profiles in the extended solar corona. *Astron. Astrophys.* **342**, 592. [ADS](#).
- Zhukov, A.N., Veselovsky, I.S., Koutchmy, S., Delannée, C.: 2000, Coronal plasmoid dynamics. II. The nonstationary fine structure. *Astron. Astrophys.* **353**, 786. [ADS](#).